

Supplement of Atmos. Chem. Phys., 20, 11625–11637, 2020
<https://doi.org/10.5194/acp-20-11625-2020-supplement>
© Author(s) 2020. This work is distributed under
the Creative Commons Attribution 4.0 License.



Supplement of

Aerosol light absorption and the role of extremely low volatility organic compounds

Antonios Tasoglou et al.

Correspondence to: Spyros N. Pandis (spyros@chemeng.upatras.gr)

The copyright of individual parts of the supplement might differ from the CC BY 4.0 License.

S1. Data analysis of TD measurements

The OA MFR is the ratio of OA concentration remaining after passing through the TD over the ambient OA concentration passing through the bypass line. The ambient OA concentrations were corrected for the AMS particle collection efficiency (CE_{amb}) calculated by the algorithm of Kostenidou et al. (2007). The average CE_{amb} value for the entire campaign was 0.64. The thermodenuded OA concentration was also corrected for the corresponding TD AMS collection efficiency (CE_{TD}) which was higher from the ambient and equal to 0.79 on average.

Figure S1 shows the collection efficiency-corrected ambient and TD OA mass concentrations. The TD temperature time series of the entire campaign is also shown. The ambient OA concentration was quite variable ranging from 0.25 to 2.5 $\mu\text{g m}^{-3}$. The average ambient OA concentration observed during this campaign (1.2 $\mu\text{g m}^{-3}$) was almost half of that during May 2008 in FAME-08 (Hildebrandt et al., 2010).

The MFR calculation assumes implicitly that the OA concentration remains constant during the measurement period. If two consecutive OA ambient mass concentrations differed by more than 25% the corresponding MFR was not included in the analysis. Also, in order to ensure that the temperature remained constant between two consecutive TD samples, the absolute difference between the two samples had to be less than 5 °C. If this difference for a TD sample was higher, then the sample was not included in our analysis.

The same quality control approach was used also for the factors resulting from the PMF analysis of the AMS spectra. However, in this case a minimum concentration threshold of 0.1 $\mu\text{g m}^{-3}$ was used for the ambient concentrations together with the criterion of the stability of the ambient concentrations during the sampling period. MFR values corresponding to concentrations of the PMF factors below this threshold were eliminated from the analysis. These criteria still allowed us to use approximately 70% of the measured values. In the present work we analyzed the complete datasets together averaging the corresponding results.

The MFR values were corrected for particle losses in the TD. These number losses inside the TD are due to diffusion of the smaller particles to the walls, or deposition of the larger particles on the TD walls, and thermophoretic losses due to temperature differences (Burtscher et al., 2001). To account for these losses, sample flow rate as well as size- and temperature-dependent loss corrections were applied following Louvaris et al. (2017) corresponding to the operating

conditions during the campaign. The final step of the data analysis was to average the corrected for CE and TD losses MFR data based on temperature bins of 10°C.

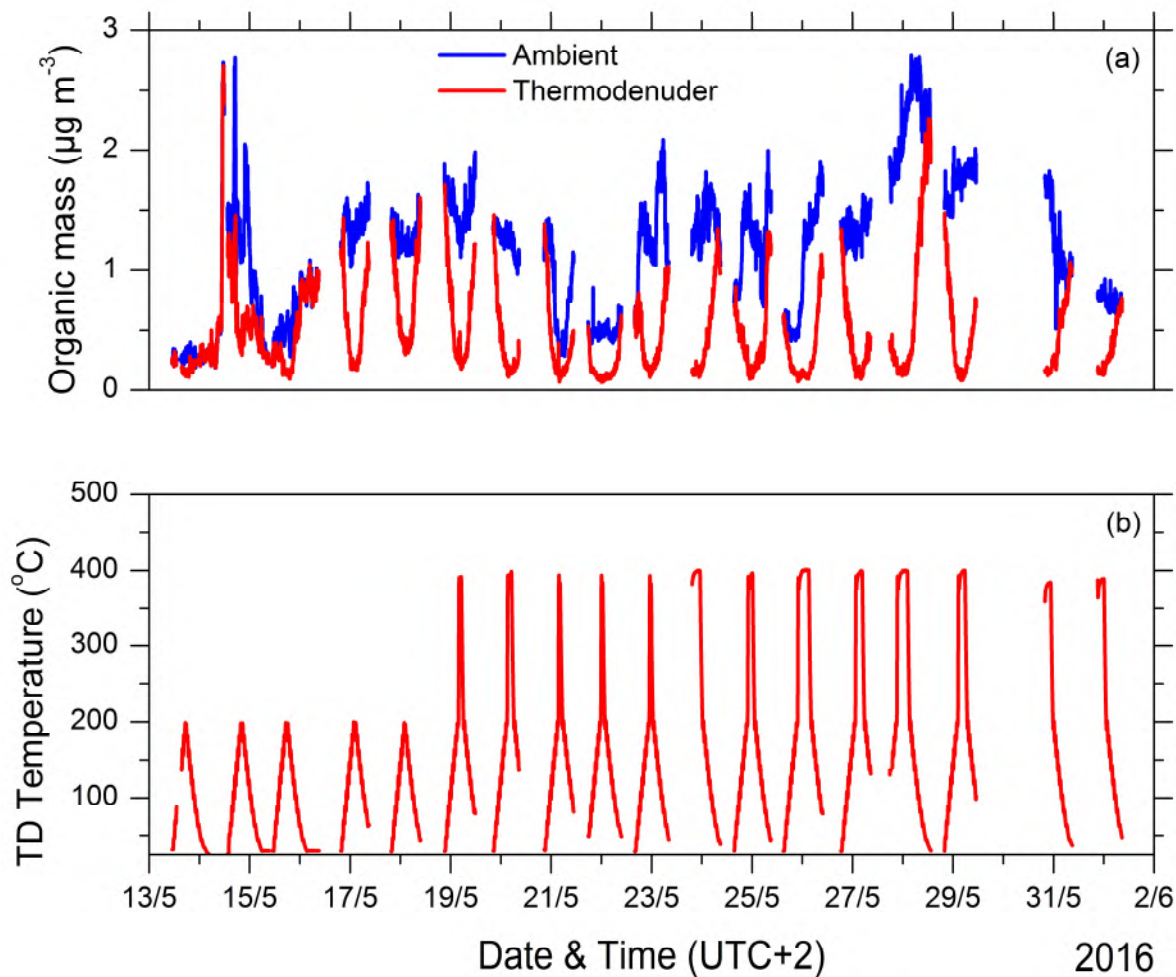


Figure S1: (a) Time series of the total ambient (blue line) and total thermodenuded (red line) OA mass concentration. (b) TD temperature during the measurement period.

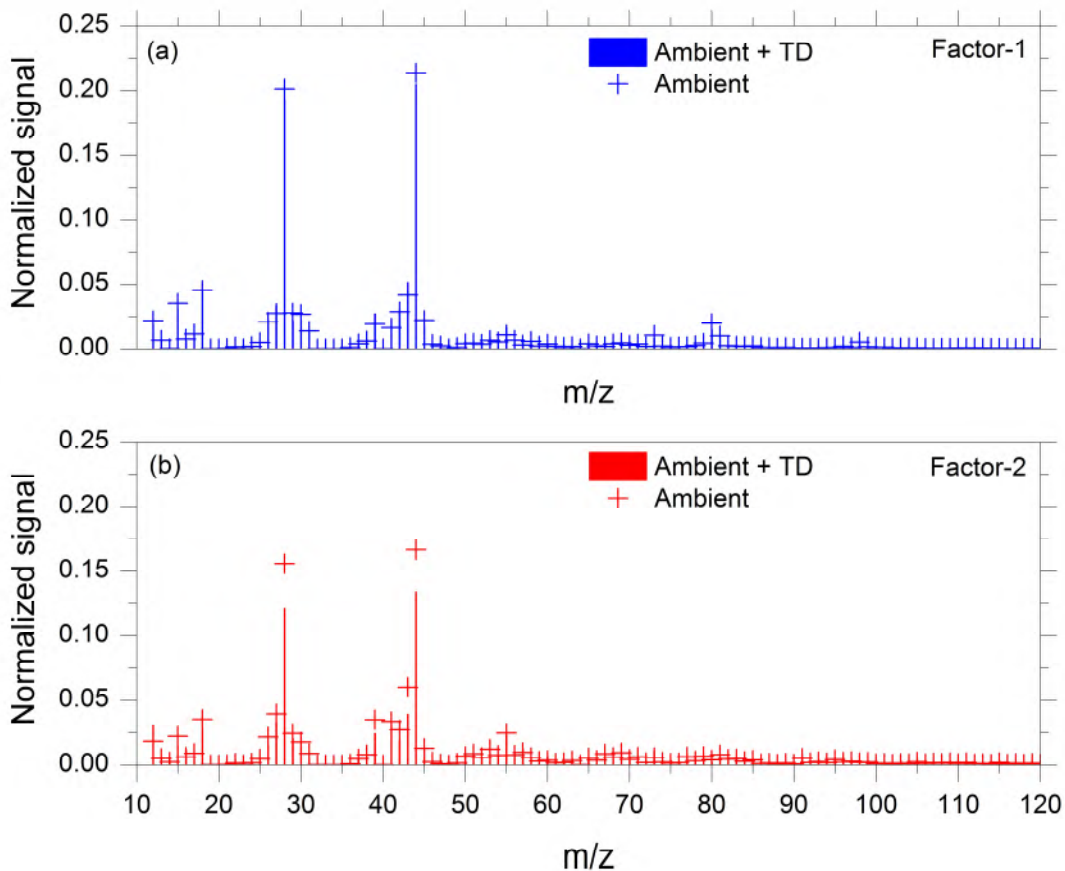


Figure S2: (a) Comparison of mass spectra of ambient OA PMF factor 1 analysis (crosses) and ambient plus thermodenuder PMF analysis (bars). (b) Comparison of mass spectra of ambient OA PMF factor 2 analysis (crosses) and ambient plus thermodenuder PMF analysis (bars).

Source apportionment of the OA was performed for the combined ambient and thermodenuded AMS spectra. This analysis was repeated by using only the ambient data, resulting in the same factors as for the complete dataset. Detailed analysis for the ambient organic components can be found in Florou et al. (in prep.). Kostenidou et al. (2009) proposed the theta angle (θ) as an indicator of mass spectra similarity by treating the AMS spectra as vectors and calculating their corresponding angle. Lower θ implies more similar spectra. Comparing the PMF results of only the ambient data and of the ambient plus TD spectra, the resulting angles were 4° for Factor 1 and 8° for Factor 2 suggesting that the ambient plus TD PMF analysis gave for all practical purposes the same factors as the ambient-only OA analysis. The ambient and TD mass spectra of the two factors are shown in Figure S2.

S2. Sensitivity analysis for the TD model

Sensitivity tests were performed in order to evaluate the behavior of the calculated volatility distributions to changes in the accommodation coefficient (a_m) and the effective vaporization enthalpy (ΔH_{vap}). First, the sensitivity of the volatility distributions to the accommodation coefficient were investigated using values ranging between 0.01 and 1. Both the volatility distribution and the effective ΔH_{vap} were recalculated, and the results were compared to the base case. The changes in the volatility distribution and the accommodation coefficient were also studied when the effective ΔH_{vap} ranged from 50 kJ mol⁻¹ to 100 kJ mol⁻¹. The same sensitivity analysis was also performed for the volatility distributions of each PMF factor.

The measured and the predicted thermograms during the sensitivity tests to a_m are shown in Figure S3. When the a_m was reduced to 0.01, the mass transfer resistances during the OA evaporation increased. In this case we assume a slower OA evaporation compared to the rest of the cases with $a_m=0.1$, $a_m=1$ or $a_m=0.27$ (base case). The changes in the estimated volatility distributions were modest. A decrease of a_m resulted in general in a small increase of the estimated SVOC content. The estimated ΔH_{vap} values were 100, 88 ± 14 , and 70 ± 19 kJ mol⁻¹ for the cases of $a_m=0.01$, 0.1, and 1.0 respectively compared to the 80 ± 20 kJ mol⁻¹ for the base case.

Figure S4 shows the predicted thermograms for ΔH_{vap} of 50 and 100 kJ mol⁻¹. For the reported base case, ΔH_{vap} was 80 ± 20 kJ mol⁻¹. The predicted thermograms for ΔH_{vap} of 50 and 100 kJ mol⁻¹ reproduced the experimental observations relatively well, but with higher error than the base case model results. The differences for these cases were more pronounced for temperatures between 150 °C and 200 °C. Once again modest changes were found in the estimated volatility distributions when ΔH_{vap} varied from 50 kJ mol⁻¹ to 100 kJ mol⁻¹. The ΔH_{vap} decrease to 50 kJ mol⁻¹ resulted in a corresponding increase of SVOCs by almost 15%. The estimated a_m showed little variability compared to the base case value of 0.27.

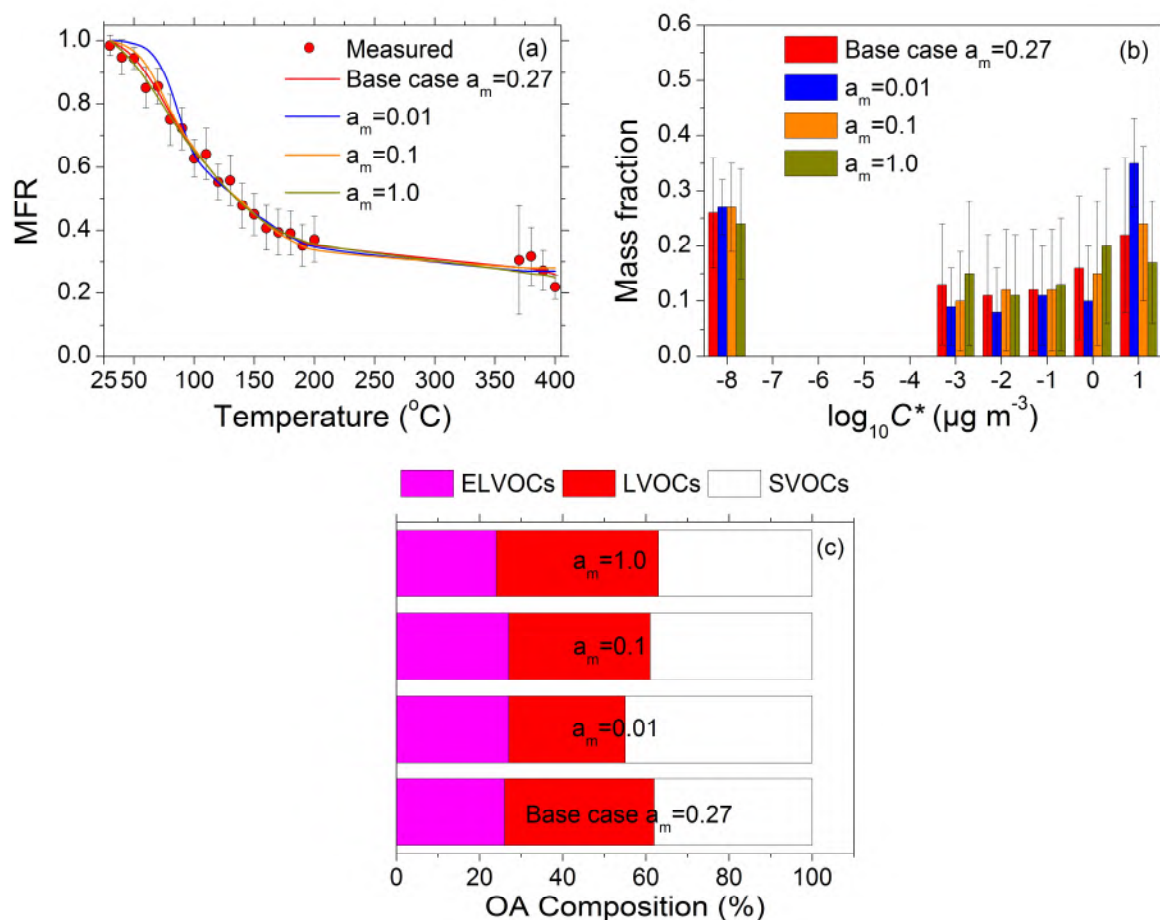


Figure S3: (a) Measured (red circles) and predicted thermograms for the base case (red line), $a_m=0.01$ (blue line), $a_m=0.1$ (orange line), and $a_m=1.0$ (dark yellow line) for total OA FAME-16 according to the model of Karnezi et al. (2014). The error bars represent ± 2 standard deviations of the mean. (b) Estimated OA volatility distributions for the base case and the sensitivity tests to different a_m values along with their corresponding uncertainties (± 1 standard deviation of the mean) according to the model of Karnezi et al. (2014). (c) OA composition for the different a_m values. ELVOCs are in magenta, LVOCs in red and SVOCs in white.

The changes in the volatility distributions for the two-factor solution obtained from the PMF analysis (MO-OOA and LO-OOA) are summarized in Figures S5 and S6. For the MO-OOA factor, when a_m was reduced to 0.01 mass transfer resistances during the evaporation increased resulting in slower evaporation of MO-OOA. The predicted thermograms were quite similar in all cases (Figure S5). The estimated ΔH_{vap} increased to 147 kJ mol^{-1} for a_m equal to 0.01 and 106 kJ mol^{-1} for a_m equal to 0.1 compared to the base case value of 89 kJ mol^{-1} .

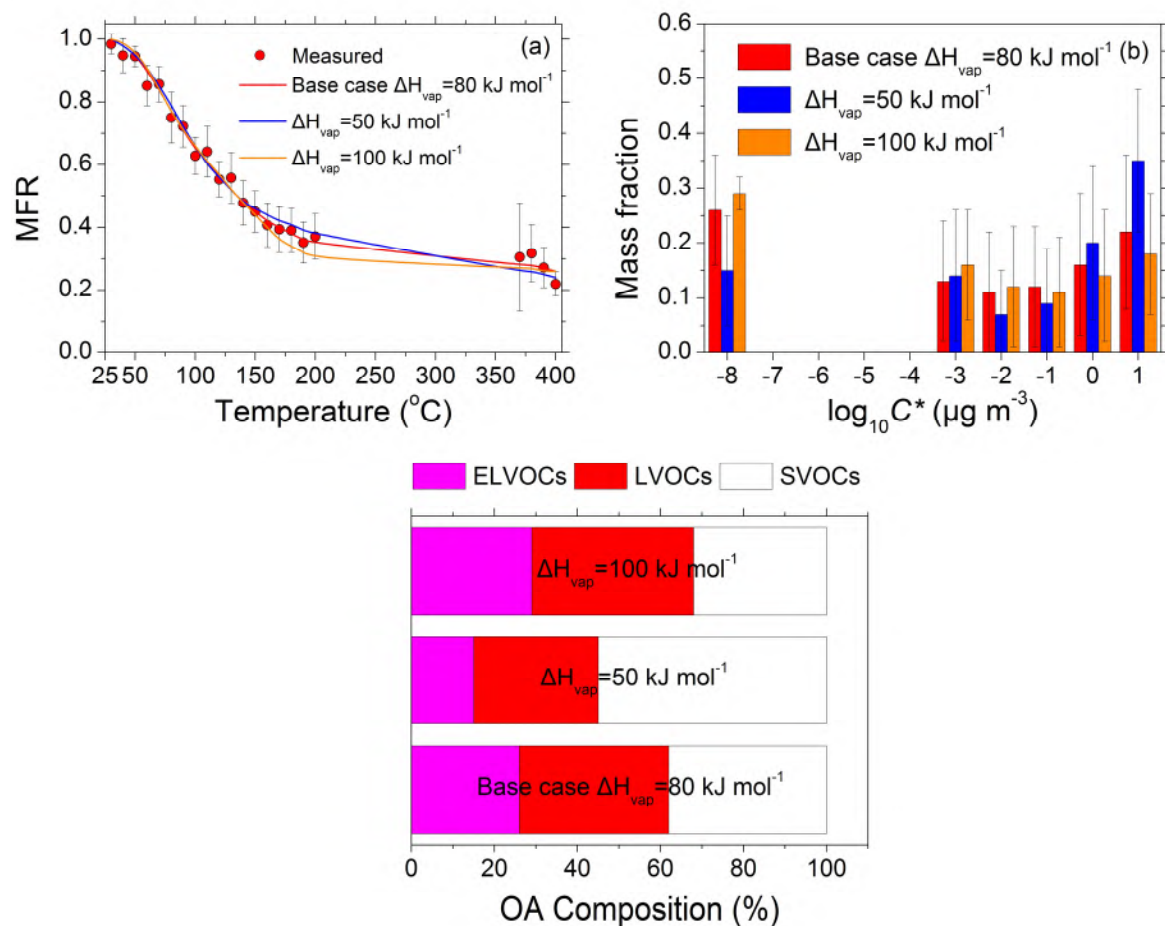


Figure S4: (a) Measured (red circles) and predicted thermograms for the base case (red line), $\Delta H_{vap} = 50 \text{ kJ mol}^{-1}$ (blue line) and $\Delta H_{vap} = 100 \text{ kJ mol}^{-1}$ (orange line) for total OA FAME-16 according to the model of Karnezi et al. (2014). The error bars represent ± 2 standard deviations of mean. (b) Estimated OA volatility distributions for the base case and the sensitivity tests to different ΔH_{vap} values along with their corresponding uncertainties (± 1 standard deviation of the mean) according to the model of Karnezi et al. (2014). (c) OA composition for the different ΔH_{vap} values. ELVOCs are in magenta, LVOCs in red and SVOCs in white.

Increasing the a_m to unity the ΔH_{vap} decreased to 71 kJ mol^{-1} . Its volatility distribution did not change significantly when a_m ranged from 0.01 to 1.0. The changes in the MO-OOA composition were modest for changing the a_m from 0.1 and 1.0 compared to the base case results. Only for the case of a_m equal to 0.01 the LVOC and ELVOC contents decreased and increased respectively by 10%. When reducing the ΔH_{vap} of the MO-OOA factor to 50 kJ mol^{-1} (base case 89 kJ mol^{-1}) the evaporation was faster after $225 \text{ }^\circ\text{C}$ compared to the other values of 100 and 150 kJ mol^{-1} (Fig. S6a). The estimated accommodation coefficient increased for increasing the ΔH_{vap} to 150 kJ mol^{-1} , whereas remained the same and increased for $\Delta H_{vap} = 100$ and 50 kJ mol^{-1} respectively. The

estimated volatility distributions were changed by 5-10% in the lower and higher volatility bins both for reducing the ΔH_{vap} to 50 kJ mol⁻¹ and for increasing it to 100 and 150 kJ mol⁻¹ compared to the base case results (Figure S6b, Table 1). The MO-OOA composition was modestly changed when increasing the ΔH_{vap} to 100 and 150 kJ mol⁻¹, where the ELVOC and SVOCs content increased by 5-10%, while the LVOCs remained almost the same. When decreasing ΔH_{vap} to 50 kJ mol⁻¹, the ELVOCs was reduced by almost 15% following the SVOCs increase by the same amount. Once again, the LVOCs remained the same amount (Figure S6c).

Table S1: Estimated volatility parameters during sensitivity tests to accommodation coefficient (a_m) and enthalpy of vaporization (ΔH_{vap}) for MO-OOA according to the model of Karnezi et al. (2014).

	$a_m = 0.01$	$a_m = 0.1$	$a_m = 1.0$	Base case $a_m=0.27$ (0.18-0.6) ^a
C^* ($\mu\text{g m}^{-3}$)		[10 ⁻⁸ 10 ⁻³ 0.01 0.1 1.0 10.0]		
Mass fraction	[0.43 0.10 0.07 0.08 0.10 0.22]	[0.35 0.14 0.07 0.08 0.12 0.24]	[0.27 0.11 0.12 0.11 0.17 0.22]	[0.30 0.12 0.10 0.10 0.13 0.25]
ΔH_{vap} (kJ mol ⁻¹)	147 ± 13	106 ± 30	71 ± 26	89 ± 35
	$\Delta H_{\text{vap}} = 50 \text{ kJ mol}^{-1}$	$\Delta H_{\text{vap}} = 100 \text{ kJ mol}^{-1}$	$\Delta H_{\text{vap}} = 150 \text{ kJ mol}^{-1}$	Base case $\Delta H_{\text{vap}} = 89 \pm 35 \text{ kJ mol}^{-1}$
C^* ($\mu\text{g m}^{-3}$)		[10 ⁻⁸ 10 ⁻³ 0.01 0.1 1.0 10.0]		
Mass fraction	[0.13 0.13 0.13 0.10 0.13 0.38]	[0.42 0.07 0.09 0.11 0.15 0.16]	[0.47 0.12 0.10 0.09 0.10 0.12]	[0.30 0.12 0.10 0.10 0.13 0.25]
a_m	0.59 (0.25-0.43) ^a	0.26 (0.17-0.52) ^a	0.09 (0.07-0.25) ^a	0.27 (0.18-0.6) ^a

^a The values in parenthesis represent the corresponding uncertainties for the estimated accommodation coefficients.

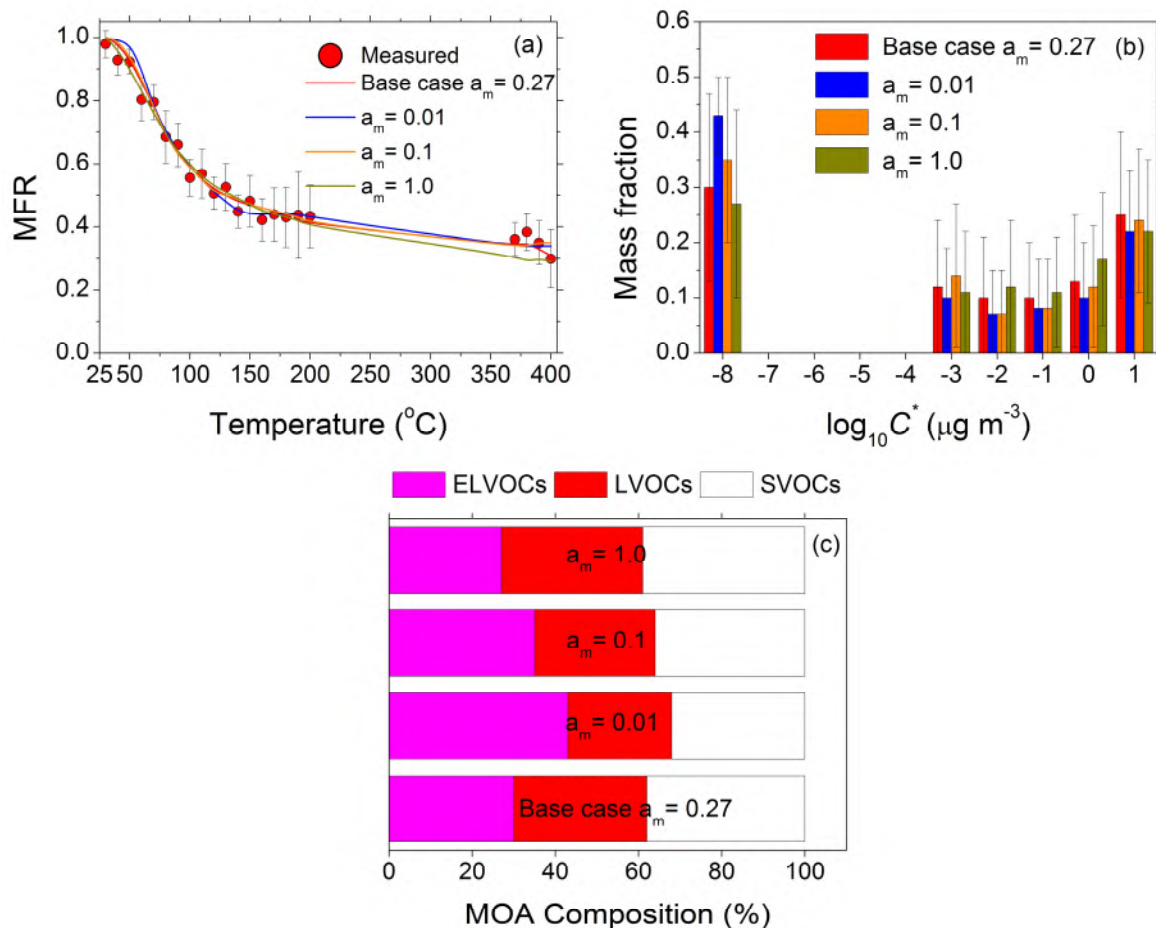


Figure S5: (a) Measured (red circles) and predicted thermograms for the base case (red line), $a_m=0.01$ (blue line), $a_m=0.1$ (orange line), and $a_m=1.0$ (dark yellow line) for MO-OOA FAME-16 according to the model of Karnezi et al. (2014). The error bars represent ± 2 standard deviations of the mean. (b) Estimated MO-OOA volatility distributions for the base case and the sensitivity tests to different a_m values along with their corresponding uncertainties (± 1 standard deviation of the mean) according to the model of Karnezi et al. (2014). (c) MO-OOA composition for the different a_m values. ELVOCs are in magenta, LVOCs in red and SVOCs in white.

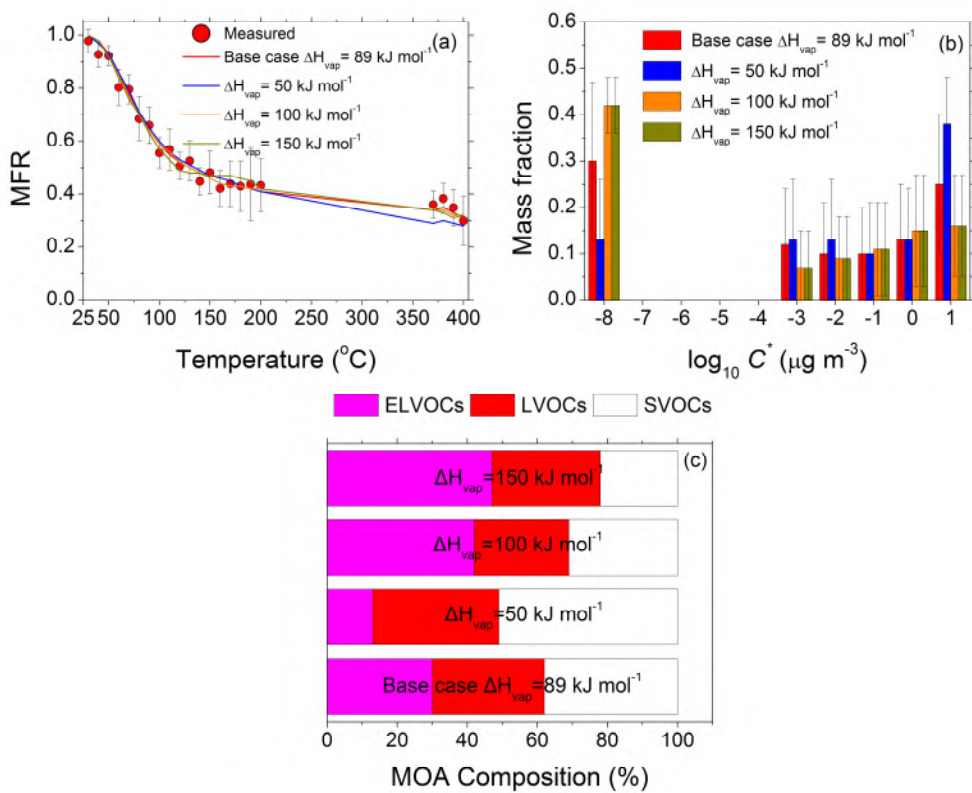


Figure S6: (a) Measured (red circles) and predicted thermograms for the base case (red line), ΔH_{vap} = 50 kJ mol⁻¹ (blue line) and ΔH_{vap} = 100 kJ mol⁻¹ (orange line) for MO-OOA FAME-16 according to the model of Karnezi et al. (2014). The error bars represent ± 2 standard deviations of mean. (b) Estimated MO-OOA volatility distributions for the base case and the sensitivity tests to different ΔH_{vap} values along with their corresponding uncertainties (± 1 standard deviation of the mean) according to the model of Karnezi et al. (2014). (c) MO-OOA composition for the different ΔH_{vap} values. ELVOCs are in magenta, LVOCs in red and SVOCs in white.

The same behavior was also obtained for the LO-OOA factor during the same test (Figure S7). The volatility distribution did not change significantly, when a_m was varied from 0.01 to unity. Its ΔH_{vap} increased also when a_m decreased to 0.01 compared to the base case value (67 kJ mol⁻¹). However, ΔH_{vap} remained almost constant for a_m equal to 0.1 and increased for a_m equal to unity. The LO-OOA composition remained similar during the a_m changes. When reducing the LO-OOA ΔH_{vap} from 67 (base case) to 50 kJ mol⁻¹, faster evaporation was observed compared both to the base case and the cases of ΔH_{vap} equal to 80 and 100 kJ mol⁻¹ (Figure S8a). The accommodation coefficient once again increased and decreased by decreasing and increasing the ΔH_{vap} ,

respectively. Modest changes of 5-10% were observed in the volatility distribution by changing ΔH_{vap} (Figure S8b, Table 2). The same changes were also observed for the LO-OOA composition. When reducing ΔH_{vap} , the ELVOC content decreased by almost 10% with a subsequent increase of the SVOCs as opposed to the increase of ΔH_{vap} (Figure S8c).

Table S2: Estimated volatility parameters during sensitivity tests to accommodation coefficient (a_m) and enthalpy of vaporization (ΔH_{vap}) for LO-OOA according to the model of Karnezi et al. (2014).

	$a_m = 0.01$	$a_m = 0.1$	$a_m = 1.0$	Base case $a_m=0.09$ (0.07-0.31) ^a
C^* ($\mu\text{g m}^{-3}$)	[10 ⁻⁸ 10 ⁻³ 0.01 0.1 1.0 10.0]			
Mass fraction	[0.20 0.15 0.11 0.14 0.22 0.18]	[0.13 0.13 0.13 0.17 0.20 0.24]	[0.14 0.16 0.11 0.16 0.28 0.15]	[0.15 0.14 0.12 0.16 0.24 0.19]
ΔH_{vap} (kJ mol ⁻¹)	89 ± 10	63 ± 15	49 ± 20	67 ± 20
	$\Delta H_{\text{vap}} = 50 \text{ kJ mol}^{-1}$	$\Delta H_{\text{vap}} = 80 \text{ kJ mol}^{-1}$	$\Delta H_{\text{vap}} = 100 \text{ kJ mol}^{-1}$	Base case $\Delta H_{\text{vap}}=67 \pm 20 \text{ kJ mol}^{-1}$
C^* ($\mu\text{g m}^{-3}$)	[10 ⁻⁸ 10 ⁻³ 0.01 0.1 1.0 10.0]			
Mass fraction	[0.09 0.11 0.12 0.14 0.29 0.25]	[0.2 0.16 0.13 0.18 0.21 0.12]	[0.25 0.22 0.12 0.17 0.17 0.07]	[0.15 0.14 0.12 0.16 0.24 0.19]
a_m	0.19 (0.13-0.37) ^a	0.05 (0.04-0.15) ^a	0.02 (0.01-0.06) ^a	0.09 (0.07-0.31) ^a

^a The values in parenthesis represent the corresponding uncertainties for the estimated accommodation coefficients.

If one assumes that the uncertainty range of the ΔH_{vap} is $\pm 35 \text{ kJ mol}^{-1}$ (except of the case of MO-OOA where a_m was 0.01 and the ΔH_{vap} was 147 kJ mol^{-1}) and of the accommodation coefficient plus or minus an order of magnitude, then the above sensitivity results can provide some reasonable uncertainty bounds of our volatility distribution estimates due to these parameters.

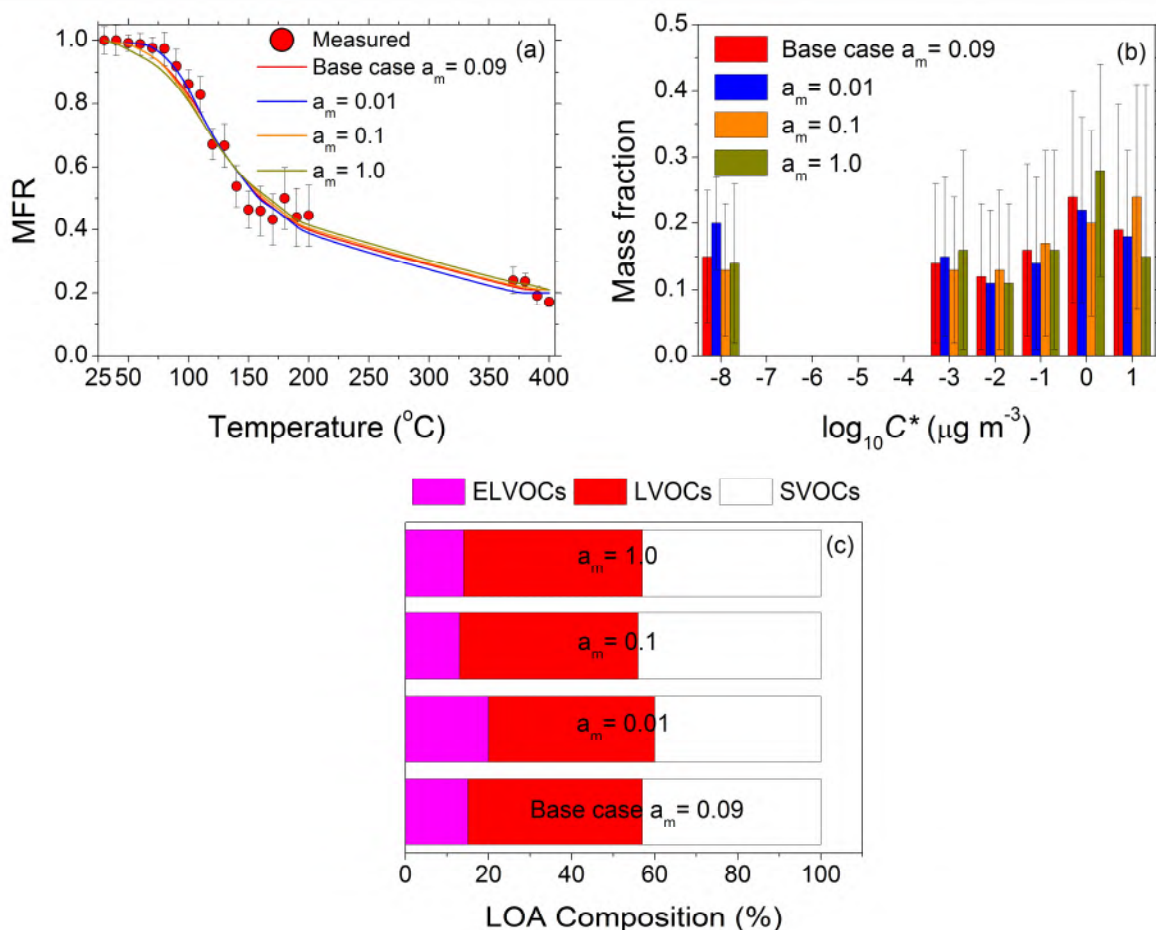


Figure S7: (a) Measured (red circles) and predicted thermograms for the base case (red line), $a_m=0.01$ (blue line), $a_m=0.1$ (orange line), and $a_m=1.0$ (dark yellow line) for LO-OOA FAME-16 according to the model of Karnezi et al. (2014). The error bars represent ± 2 standard deviations of the mean. (b) Estimated LO-OOA volatility distributions for the base case and the sensitivity tests to different a_m values along with their corresponding uncertainties (± 1 standard deviation of the mean) according to the model of Karnezi et al. (2014). (c) LO-OOA composition for the different a_m values. ELVOCs are in magenta, LVOCs in red and SVOCs in white.

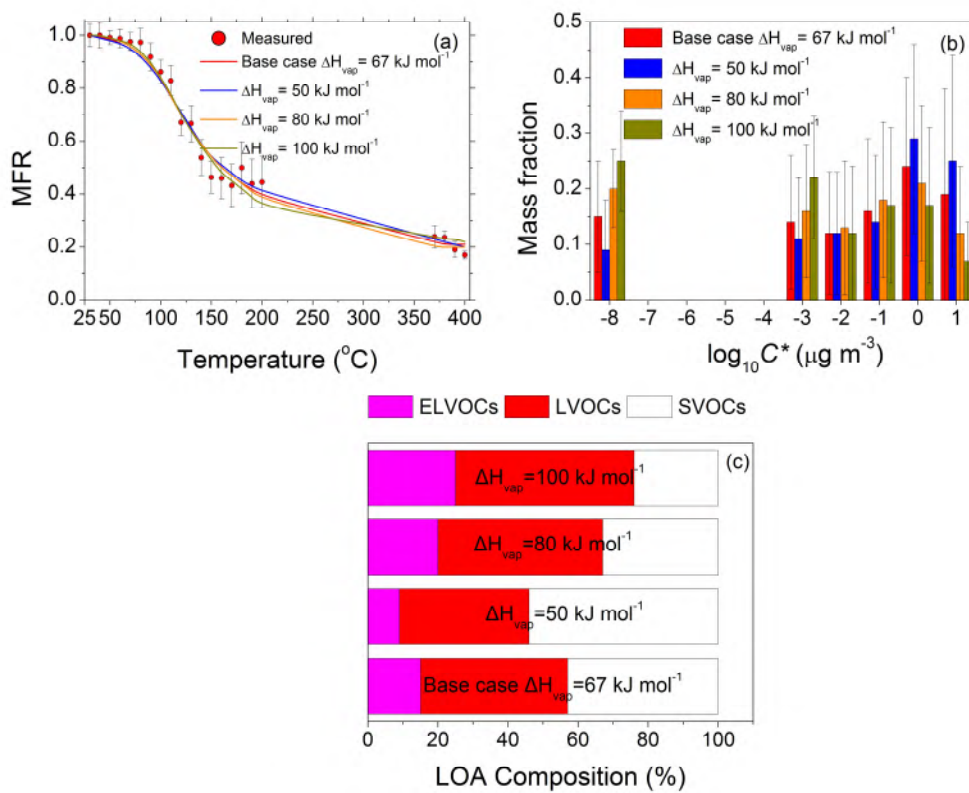


Figure S8: (a) Measured (red circles) and predicted thermograms for the base case (red line), $\Delta H_{\text{vap}} = 50 \text{ kJ mol}^{-1}$ (blue line) and $\Delta H_{\text{vap}} = 100 \text{ kJ mol}^{-1}$ (orange line) for LO-OOA FAME-16 according to the model of Karnezi et al. (2014). The error bars represent ± 2 standard deviations of mean. (b) Estimated LO-OOA volatility distributions for the base case and the sensitivity tests to different ΔH_{vap} values along with their corresponding uncertainties (± 1 standard deviation of the mean) according to the model of Karnezi et al. (2014). (c) LO-OOA composition for the different ΔH_{vap} values. ELVOCs are in magenta, LVOCs in red and SVOCs in white.

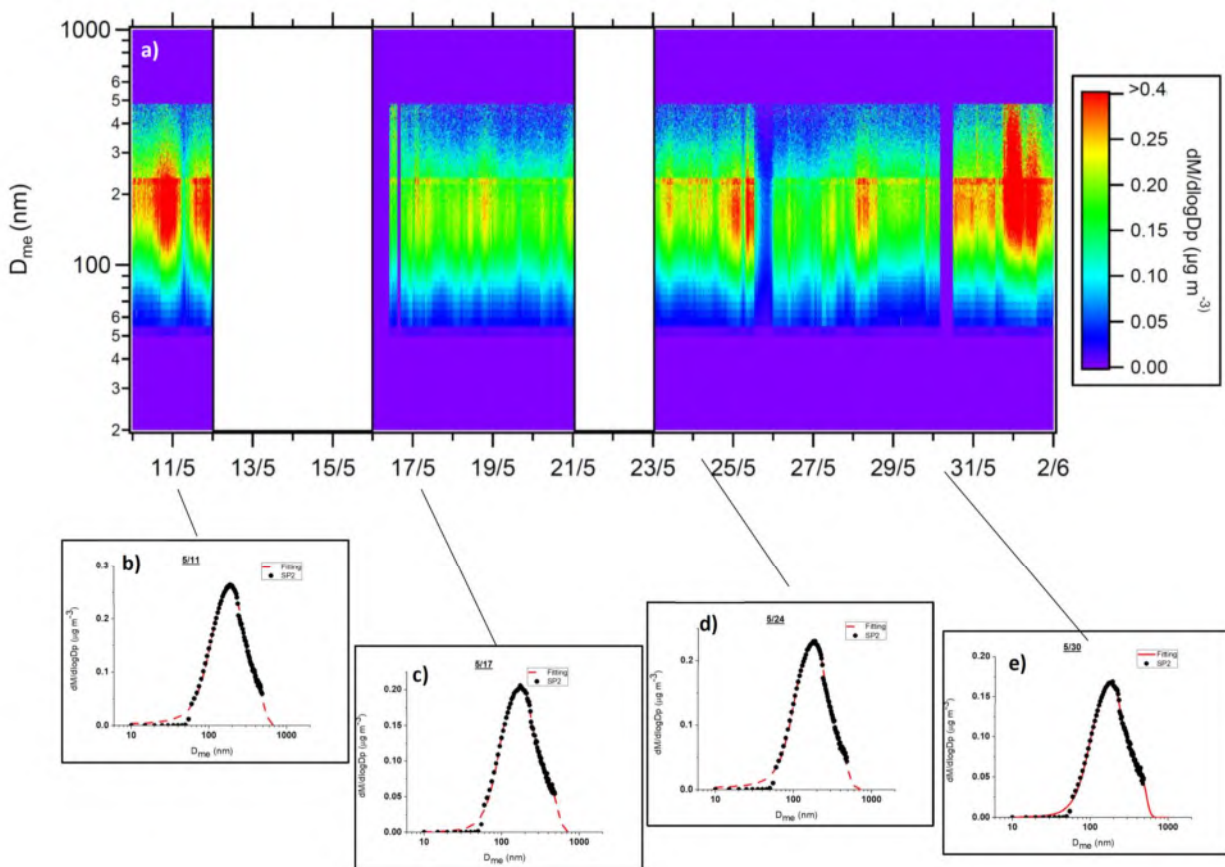


Figure S9: a) The BC mass size distributions measured as a function of time and diameter. Also shown the daily averaged size distributions on b) May/11, c) May/17, d) May/24, e) May/30 (with black dots) and the log-normal distribution fitting (red dashed lines).

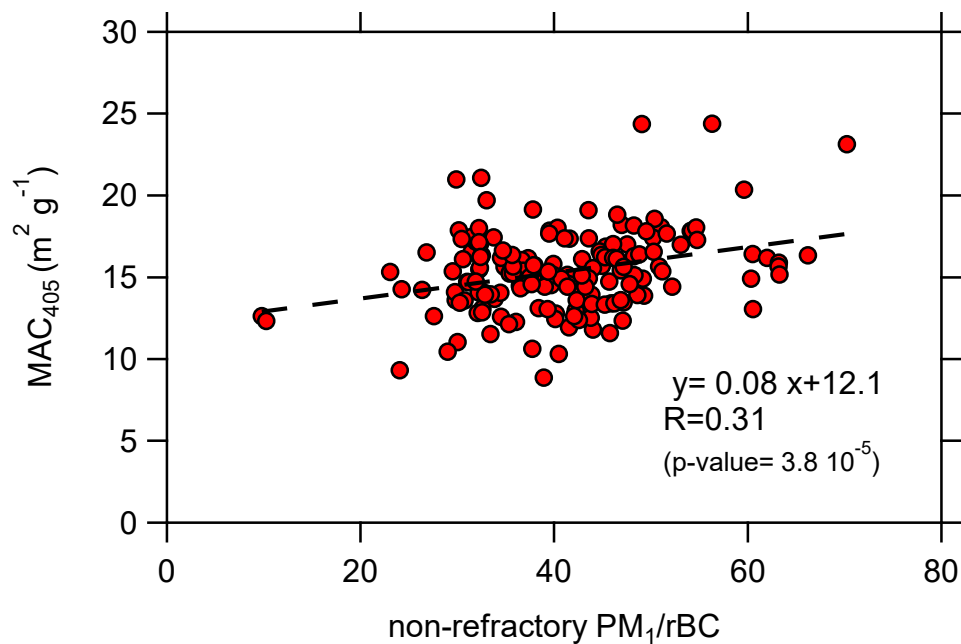


Figure S10: The MAC₄₀₅ as a function of the ratio of non-refractory PM₁ mass over the rBC mass.

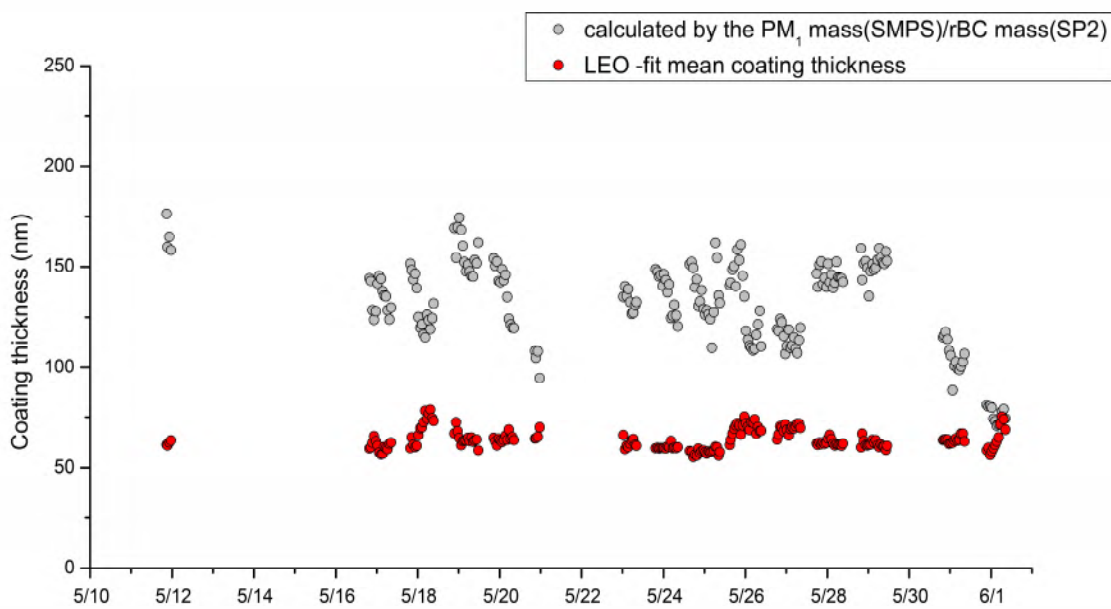


Figure S11: The coating thickness calculated by the ratio of the total aerosol mass over the rBC Mass (grey) and by the SP2 LEO fit method (red).

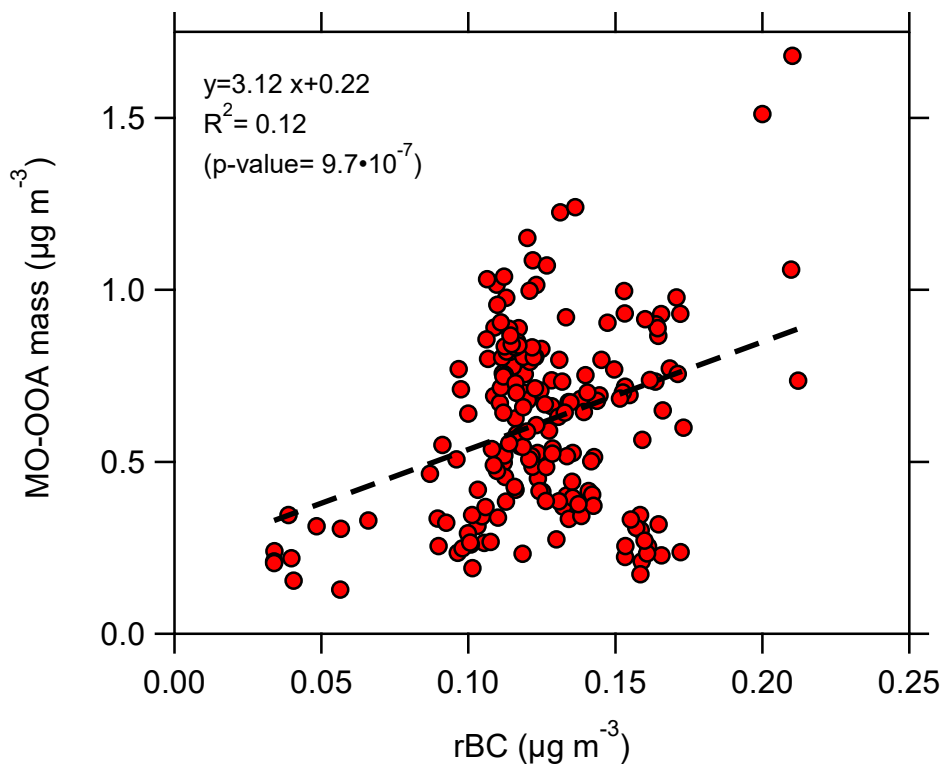


Figure S12: The MO- OOA mass as a function of the rBC mass.

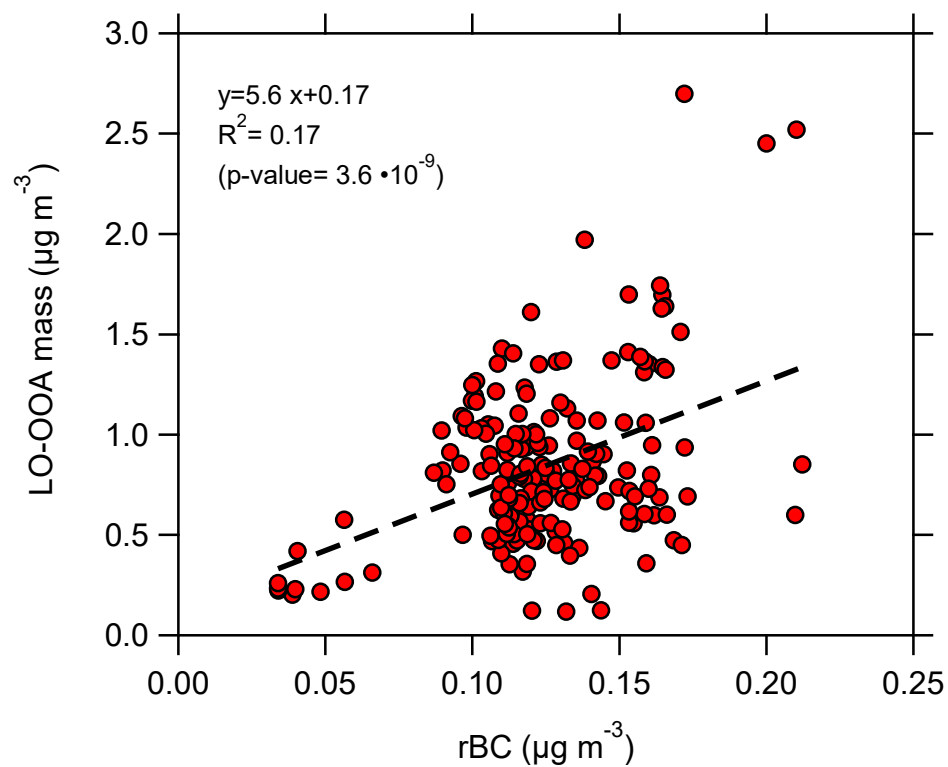


Figure S13: The LO- OOA mass as a function of the rBC mass.

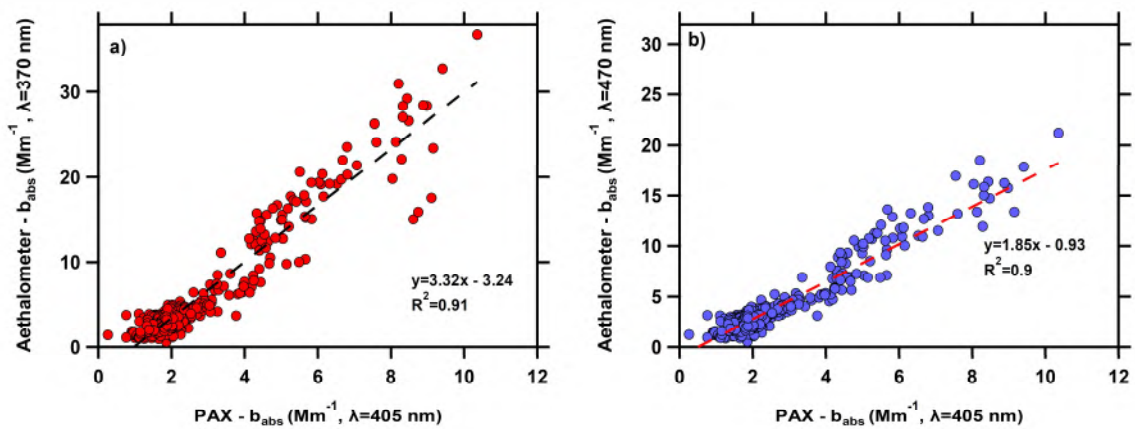


Figure S14: Comparison of the b_{abs} measured by the PAX at $\lambda=405$ nm with the b_{abs} measured by aethalometer at a) $\lambda=370$ nm and b) $\lambda=470$ nm. The dashed lines represent the linear fitting.

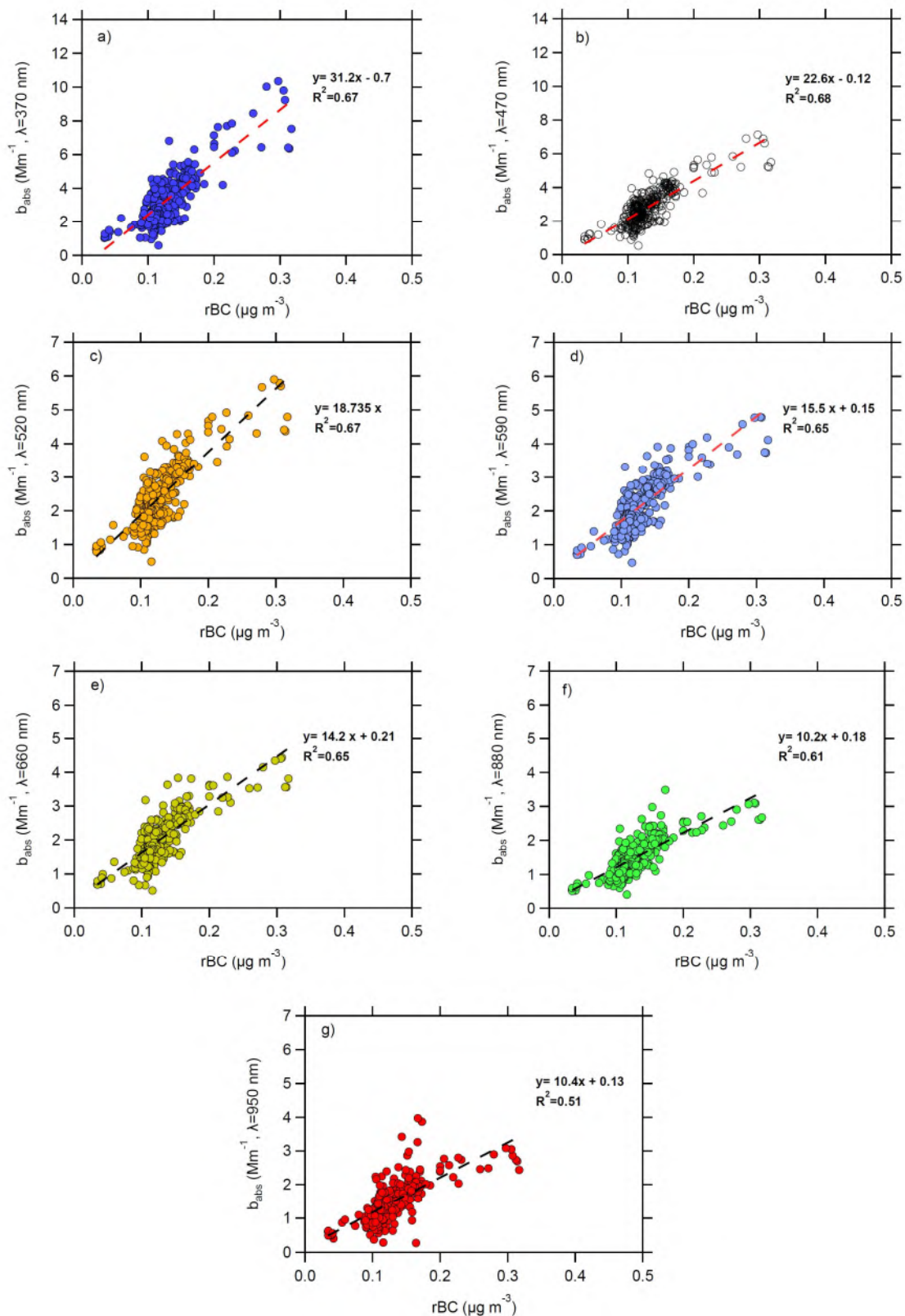


Figure S15: The absorption coefficient measured by the aethalometer in 370, 470, 520, 590, 660, 880 and 950 nm as a function of the measured rBC.

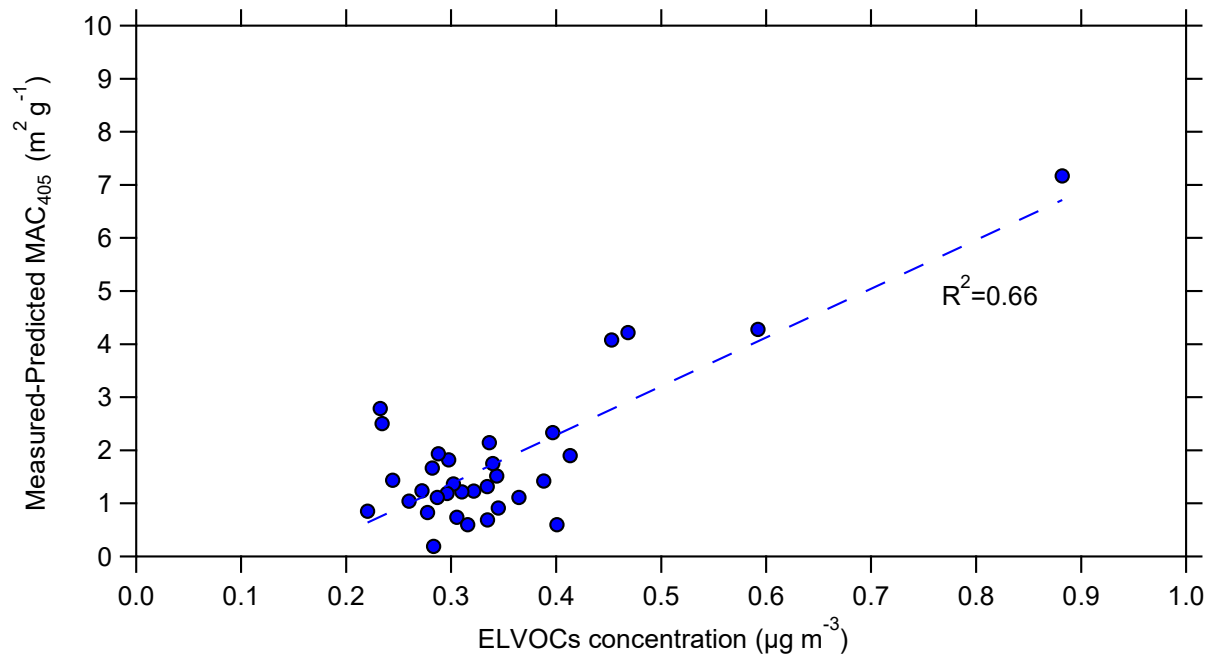


Figure S16: The difference between the measured and the predicted MAC₄₀₅ as a function of the estimated concentration of the ELVOCs. The data shown represent 3-hours averaged values.

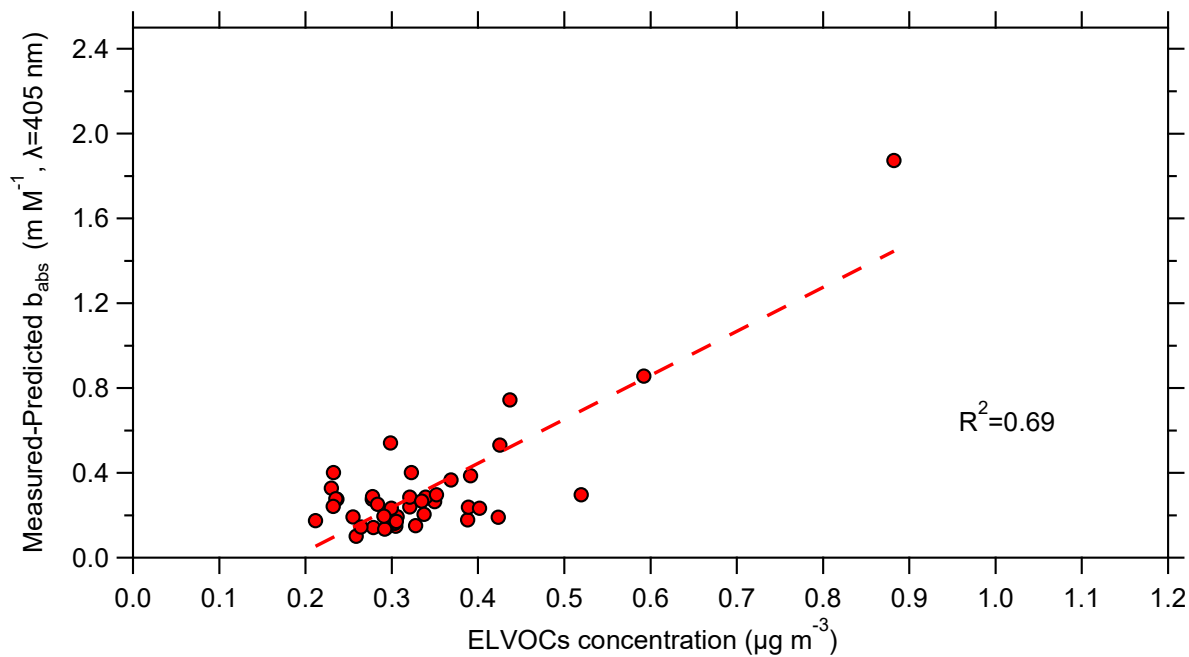


Figure S17: The unexplained absorption as a function of the estimated concentration of the ELVOCs. The predicted absorption was calculated assuming based assuming BC coating based on the LEO calculations. The data shown represent 3-hour averaged values.

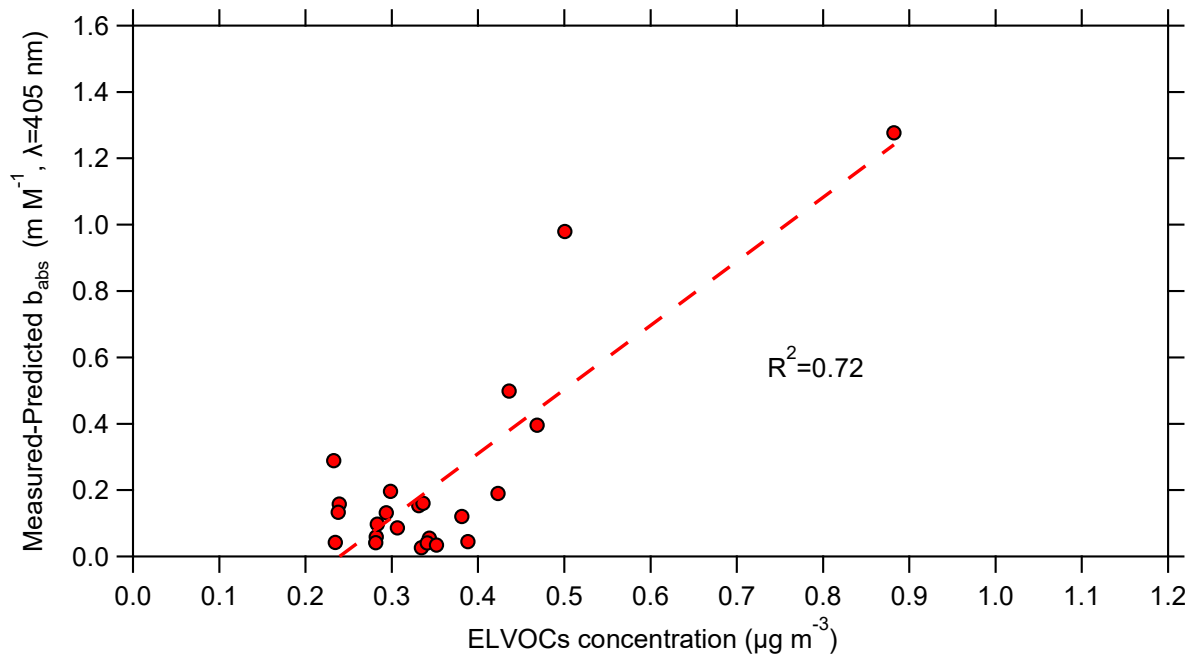


Figure S18: The unexplained absorption as a function of the estimated concentration of the ELVOCs. The predicted absorption was calculated assuming $n_{\text{rBC,high}} = 1.95 + 0.79i$. The data shown represent 3-hour averaged values.

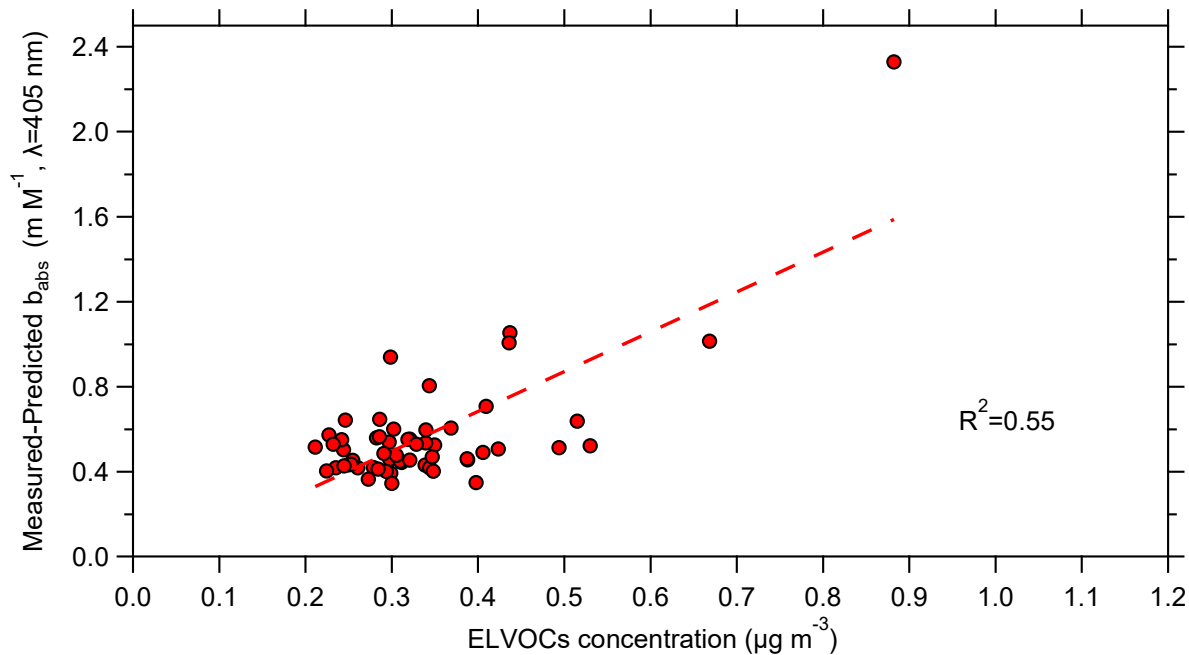


Figure S19: The unexplained absorption as a function of the estimated concentration of the ELVOCs. The predicted absorption was calculated assuming $n_{\text{rBC,low}} = 1.5 + 0.5i$. The data shown represent 3-hour averaged values.

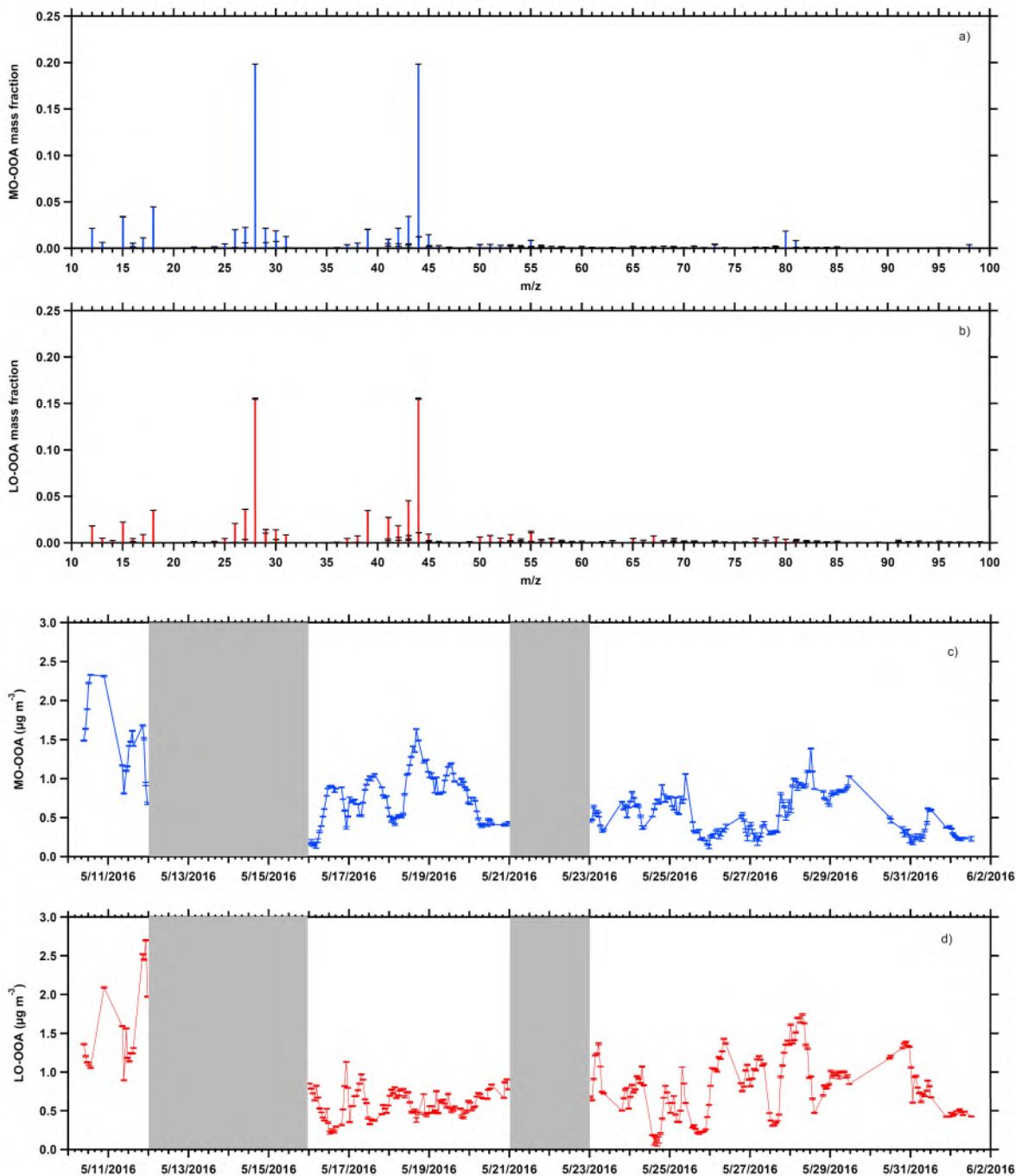


Figure S20: Results from bootstrapping the 2 factors PMF solution. The mass spectra of the average factors a) MO-OOA (blue) and b) LO-OOA (red). The error bars indicate the 1 standard deviation. The timeseries of the average factors c) MO-OOA (blue) and d) LO-OOA (red). The 1 standard deviation variation bars for each point are also shown. The shaded areas represent the dust event periods.

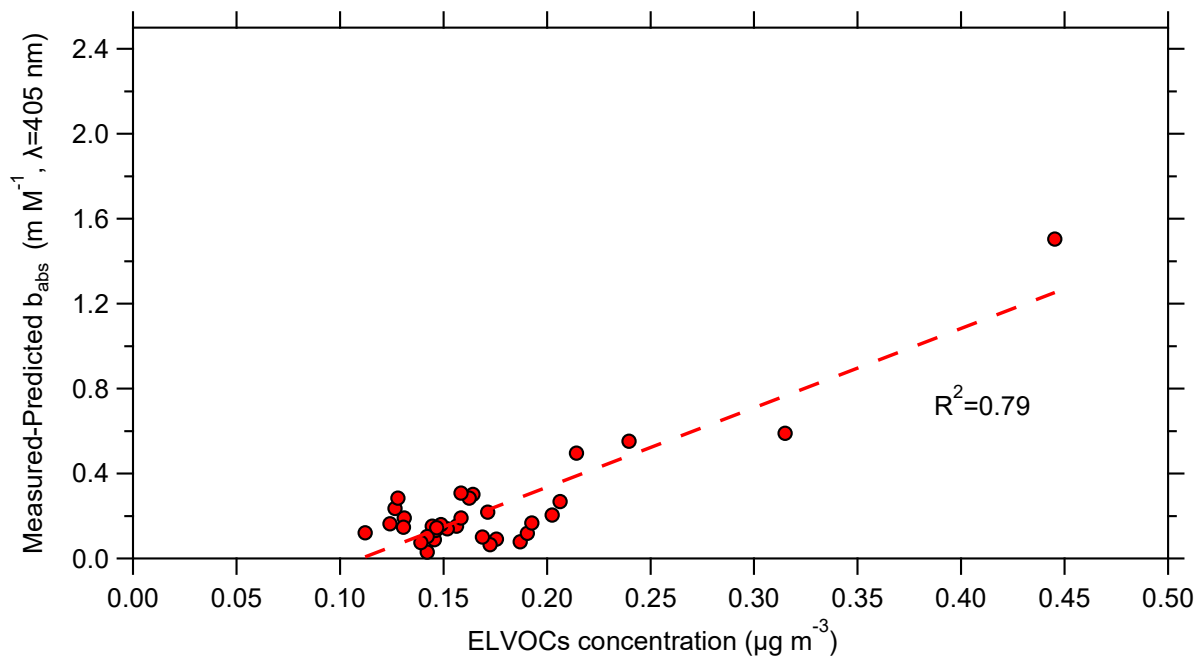


Figure S21: The unexplained absorption as a function of the low limit of the estimated concentrations of the ELVOCs. The data shown represent 3-hours averaged values.

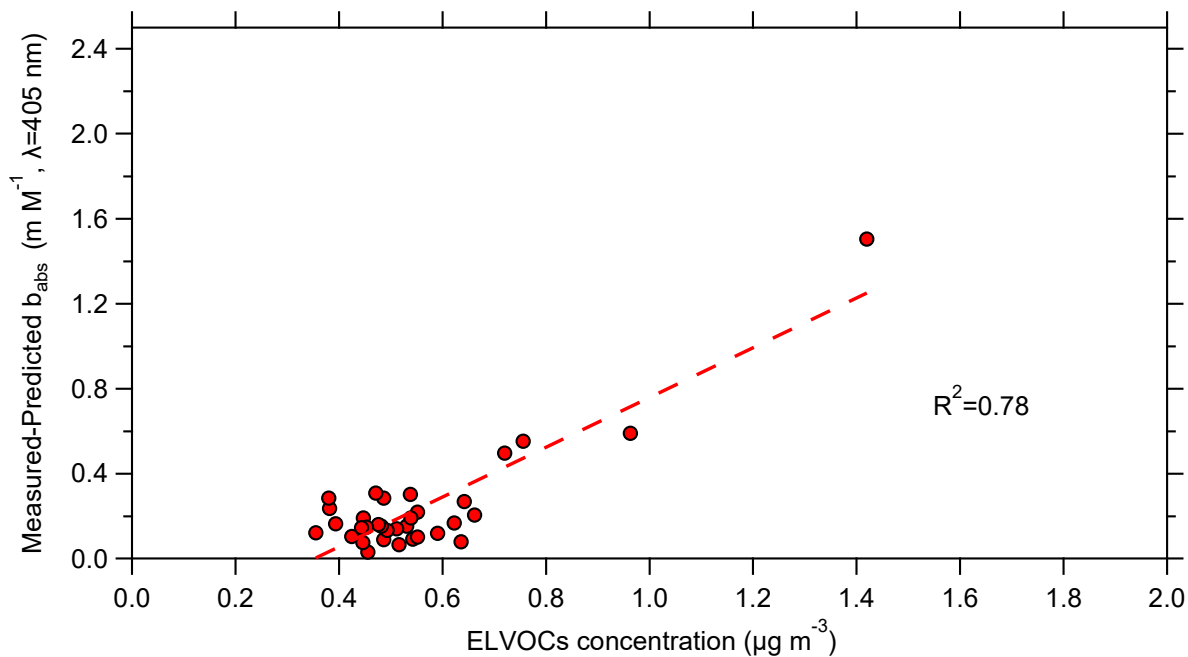


Figure S22: The unexplained absorption as a function of the high limit of the estimated concentrations of the ELVOCs. The data shown represent 3-hours averaged values.

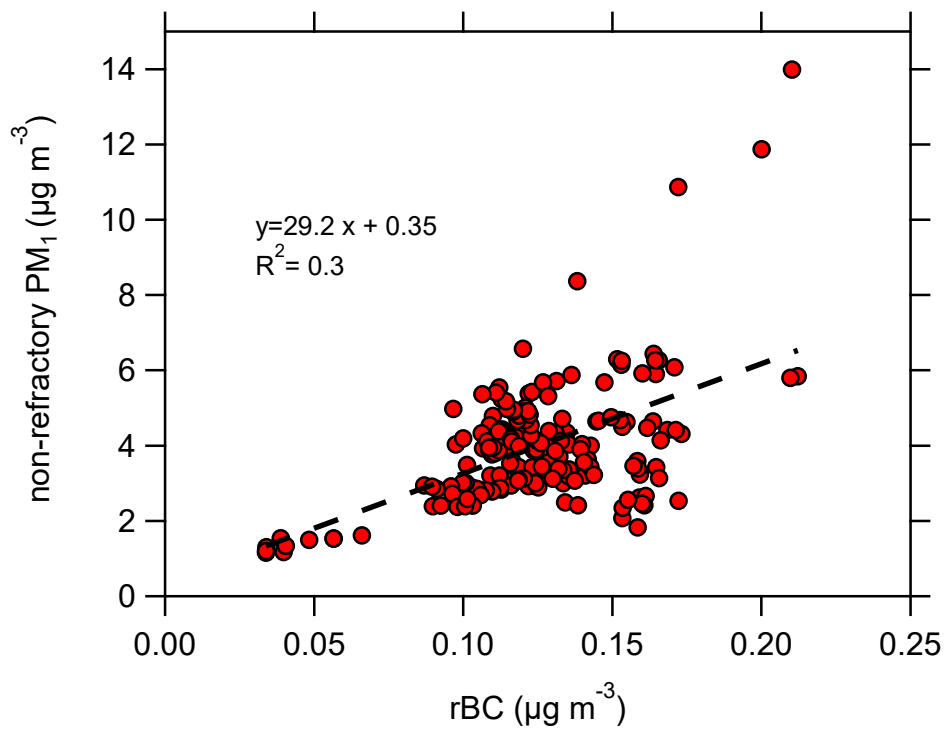


Figure S23: The non-refractory PM_{10} mass as a function of the rBC mass.

References

- Burtscher, H., Baltensperger, U., Bukowiecki, N., Cohn, P., Hüglin, C., Mohr, M., Matter, U., Nyeki, S., Schmatloch, V., Streit, N. and Weingartner, E.: Separation of volatile and non-volatile aerosol fractions by thermodesorption: Instrumental development and applications, *J. Aerosol Sci.*, 32, 427–442, 2001.
- Florou, K., Liangou, A., Louvaris, E., Kaltsonoudis, C., Tasoglou, A., Patoulias, D., Kouvarakis, G., Vlachou, A., Kourtchev, I. and Spyros N. Pandis, S. N.; The Finokalia Aerosol Measurement Experiment (FAME-16): Atmospheric processing of organic aerosol in the Eastern Mediterranean, in prep.
- Hildebrandt, L., Engelhart, G. J., Mohr, C., Kostenidou, E., Lanz, V. A., Bougiatioti, A., DeCarlo, P. F., Prévôt, A. S. H., Baltensperger, U., Mihalopoulos, N., Donahue, N. M., and Pandis, S. N.: Aged organic aerosol in the eastern Mediterranean: The Finokalia aerosol measurement experiment 2008, *Atmos. Chem. Phys.*, 10, 4167–4186, 2010.
- Karnezi, E., Riipinen, I., and Pandis, S. N.: Measuring the atmospheric organic aerosol volatility distribution: a theoretical analysis, *Atmos. Meas. Tech.*, 7, 2953–2965, doi:10.5194/amt7-2953-2014, 2014.
- Kostenidou, E., Lee, B. H., Engelhart, G. J., Pierce, J. R. and Pandis, S. N.: Mass spectra deconvolution of low, medium, and high volatility biogenic secondary organic aerosol, *Environ. Sci. Technol.*, 43, 4884–4889, 2009.
- Kostenidou, E., Pathak, R. K., and Pandis, S. N.: An algorithm for the calculation of secondary organic aerosol density combining AMS and SMPS data, *Aerosol Sci. Tech.*, 41, 1002–1010, 2007.
- Louvaris, E.E., Florou, K., Karnezi, E., Papanastasiou, D.K., Gkatzelis, G.I., and Pandis, S.N.: Volatility of source apportioned wintertime organic aerosol in the city of Athens, *Atmos. Environ.*, 158, 138-147, 2017.